Global satellite data highlights the diurnal asymmetry of the surface temperature response to deforestation

Natalie M. Schultz[1] (iD)**, Peter J. Lawrence[2]** (iD)**, and Xuhui Lee[1,3]** (iD)

[1]School of Forestry and Environmental Studies, Yale University, New Haven, Connecticut, USA, [2]Climate and Global Dynamics Division, National Center for Atmospheric Research, Boulder, Colorado, USA, [3]Yale-NUIST Center on Atmospheric Environment, Nanjing University of Information Science and Technology, Nanjing, Jiangsu, China

Abstract Uncertainties remain about the spatial pattern and magnitude of the biophysical effects of deforestation. In particular, a diurnal asymmetry in the magnitude and sign of the surface temperature response to deforestation (ΔT_S) has been observed, but the biophysical processes that contribute to day and nighttime ΔT_S are not fully understood. In this study, we use a space-for-time approach with satellite and reanalysis data to investigate the biophysical processes that control the day and nighttime ΔT_S. Additionally, we incorporate flux-tower data to examine two hypotheses for nighttime forest warming relative to open lands: (1) that forests generate turbulence in the stable nocturnal boundary layer, which brings heat aloft down to the surface, and (2) that forests store more heat during the day and release it at night. Our results confirm a diurnal asymmetry in ΔT_S. Over most regions of the world, deforestation results in daytime warming and nighttime cooling. The strongest daytime warming is in the tropics, where the average ΔT_S is 4.4 ± 0.07 K. The strongest nighttime cooling is observed in the boreal zone, where open lands are cooler than forests by an average of 1.4 ± 0.04 K. Daytime patterns of ΔT_S are explained by differences in the latent heat flux (ΔLE) and absorbed solar radiation (ΔK_a). We find that nighttime ΔT_S is related to the strength of the nocturnal temperature inversion, with stronger temperature inversions at high latitudes and weak inversions in the tropics. Forest turbulence at night combined with stored heat release drives nighttime ΔT_S patterns.

1. Introduction

Forests influence climate through the exchange of carbon dioxide, energy, and water vapor with the atmosphere [*Bonan*, 2008; *Mahmood et al.*, 2014; *Pielke et al.*, 1998]. Land cover change, in the form of deforestation, alters the terrestrial carbon cycle and surface biophysical processes [*Bala et al.*, 2007]. In contrast to changes in the global carbon cycle, the climate impacts of changes in biophysical processes tend to be more important at the local or regional scale [*Alkama and Cescatti*, 2016; *Bonan*, 2008; *Jackson et al.*, 2008]. The biophysical effects of deforestation influence surface temperature and include changes in albedo, roughness, and evapotranspiration (ET) [*Lee et al.*, 2011; *Li et al.*, 2015]. On the one hand, forests have a low albedo compared to deforested or open lands, particularly in high latitudes where they can mask the high albedo of snow [*Betts*, 2000]. On the other hand, forests are more efficient at removing heat from the surface due to their larger surface roughness [*Lee et al.*, 2011], and in humid climates, through a higher latent heat flux [*Anderson et al.*, 2011].

Until recently, much of our knowledge about the biophysical effects of deforestation came from sensitivity experiments with global climate models, with one simulation serving as a control against another with contrasting forest cover [e.g., *Lawrence and Chase*, 2010]. Model results tend to agree that the albedo effect dominates at high latitudes, resulting in a local cooling from deforestation and that a reduction in ET from deforestation in the tropics results in local warming [*de Noblet-Ducoudré et al.*, 2012]. However, there are inconsistencies in the sign, magnitude, and spatial distribution of the biophysical effects between models, some of which may be due to the differences in the parameterizations of different land cover types and the implementation of land cover change in land models [*de Noblet-Ducoudré et al.*, 2012; *Pitman et al.*, 2009]. In particular, the modeling results of deforestation tend to be inconsistent with observations in temperate forests. In contrast to the observational study of *Wickham et al.* [2013], who showed that surface temperature declines as forest extent increases, most models show that temperate forests are a source of heat relative to other types of land cover. Additional uncertainties may result from the paired simulation approach, in which biophysical effects need to be distinguished from unforced model variability or the non-local effects of land cover change, such as changes to ocean or atmospheric circulation [*Pielke et al.*, 2011]. To

remove these additional uncertainties from paired simulations, a subgrid modeling approach has been proposed as a means to isolate the biophysical effects of deforestation or other land use change within a global climate model [*Malyshev et al.*, 2015; *Schultz et al.*, 2016]. *Winckler et al.* [2017] used a complementary approach to distinguish local versus nonlocal effects of land cover change on local climate by selectively changing land surface properties in selected grid cells, while leaving the surrounding grids unchanged.

Observational methods of the biophysical effects are needed to constrain model results and reduce the uncertainty of model ensembles [*Alkama and Cescatti*, 2016]. Global or regional observational studies of the biophysical effects of deforestation or land use change have used a space-for-time approach, comparing the surface temperature of different land cover types within close proximity to each other, assuming differences in the environmental or atmospheric conditions are negligible [*Lee et al.*, 2011; *Li et al.*, 2015; *Peng et al.*, 2014; *Zhang et al.*, 2014]. An alternative approach was developed to investigate the biophysical climate effects of regions that had recent forest gains or losses [*Alkama and Cescatti*, 2016].

In situ measurements have shown that the biophysical effects of deforestation on surface air temperature follow a latitudinal pattern. Across North and South America, the temperature effect from deforestation changes from net warming to net cooling around 35°N [*Lee et al.*, 2011]. A similar pattern is observed in East Asia, with net cooling observed in site pairs north of 35.5°N [*Zhang et al.*, 2014]. Interestingly, each of these studies found that a diurnal asymmetry exists in the biophysical effect and that the diurnal temperature range is reduced with forest cover. In northern sites (>45°N), the net cooling from deforestation is driven by minimum temperature differences, with similar temperatures observed between the open and forest sites during midday [*Lee et al.*, 2011; *Zhang et al.*, 2014]. The opposite is true in the tropics (15°S to 20°N), where the net warming from deforestation is largely a result of a difference in maximum air temperature, with similar temperatures observed overnight [*Zhang et al.*, 2014].

One proposed hypothesis for the nighttime warming of forests in high latitudes is that the presence of trees causes turbulence, bringing heat from aloft to the surface during stable atmospheric conditions [*Lee et al.*, 2011]. At night, as the surface cools due to longwave emission, an inversion develops and the surface layer becomes stable, inhibiting vertical and horizontal mixing. Strong nocturnal inversions are common in dry or desert environments because the radiative cooling is unrestricted, whereas weak inversions are expected under humid or cloudy conditions. As a radiation inversion develops, turbulence is diminished in the mixed-layer, and only roughness-generated turbulence persists near the surface [*Oke*, 1987]. Indeed, it has been shown that wind turbine-enhanced vertical mixing produces local nighttime surface warming [*Zhou et al.*, 2012].

The spatial patterns of the biophysical effects of deforestation and afforestation from satellite data are in general agreement with the in situ and modeled results [*Li et al.*, 2015]. Satellite data analyses show that the daytime cooling by forests in low latitudes is driven by higher ET, while the daytime warming in high latitudes is driven by a lower albedo [*Li et al.*, 2015; *Peng et al.*, 2014]. Nighttime warming of forests follows a latitudinal pattern, with strong warming in high latitudes, and minimal differences in nighttime temperature between forests and open lands in the tropics [*Li et al.*, 2015]. During the nighttime, albedo is irrelevant and ET is generally negligible, yet observed annual mean nighttime land surface temperature differences are as large as 2 K [*Li et al.*, 2015]. An alternative hypothesis to explain nighttime warming of forests is the release of heat energy stored during the day, related to the low albedo of the forests [*Michiles and Gielow*, 2008; *Peng et al.*, 2014]. *Peng et al.* [2014] found that there was reduced nighttime warming where forests had a larger ET relative to the excess absorbed solar radiation, suggesting that nighttime warming reflects the release of daytime heat storage.

In this study, our overall goal is to investigate the biophysical drivers of the day and nighttime surface temperature response to deforestation. We extend the work of *Li et al.* [2015] by incorporating reanalysis data sets and in situ observations from flux tower sites into a satellite data-based analysis. We quantify and compare the relative strength of biophysical effects from a surface energy balance perspective. Additionally, as we are particularly interested in exploring the drivers of the nighttime response to deforestation, we investigate two complementary hypotheses that have been proposed for nighttime forest warming: (1) turbulence in a stably stratified atmospheric boundary layer, and (2) heat release from daytime heat storage. To the best of our knowledge, the near surface inversion pattern across latitude, and its relation to land surface temperature, has not yet been investigated.

Table 1. The Details of the Flux Tower Sites[a]

Site Name	Site ID	Lat (°N)	Lon (°E)	Land Cover	Γ (K)	Reference
Grasslands						
Rollesbroich	DE-RuR	50.62	6.30	GRA	−1.78	*Post et al.* [2015]
Fort Peck	US-FPe	48.31	−105.10	GRA	−1.82	*Thompson et al.* [2011]
KUOM Turfgrass Field	US-KUT	45.00	−93.19	GRA	−3.45	*Hiller et al.* [2010]
Brookings	US-Bkg	44.35	−96.84	GRA	−1.36	*Gilmanov et al.* [2005]
Canaan Valley	US-CaV	39.06	−79.42	GRA	−2.16	*Wilson and Meyers* [2007]
Vaira Ranch	US-Var	38.41	−120.95	GRA	−1.98	*Xu and Baldocchi* [2004]
Duke Forest—Open Field	US-Dk1	35.97	−79.09	GRA	−2.29	*Novick et al.* [2004]
Sevilleta Grassland	US-Seg	34.36	−106.71	GRA	−2.43	*Anderson-Teixeira et al.* [2011]
Goodwin Creek	US-Goo	34.25	−89.87	GRA	−2.81	*Wilson and Meyers* [2007]
Walnut Gulch Kendall Grasslands	US-Wkg	31.74	−109.94	GRA	−2.99	*Krishnan et al.* [2012]
Audubon Research Ranch	US-Aud	31.59	−110.51	GRA	−2.66	*Krishnan et al.* [2012]
Santarem-Km77-Pasture	BR-Sa2	−3.01	−54.54	CRO	−0.11	*Sakai et al.* [2004]
Fazenda Nossa Senhora Cattle Ranch	n/a	−10.75	−62.37	GRA	−0.14	*von Randow et al.* [2004]
Sturt Plains	AU-Stp	−17.15	133.35	GRA	−1.22	*Beringer* [2013]
Arcturus Emerald	AU-Emr	−23.86	148.47	GRA	−1.71	*Schroder* [2014]
Forests						
Western Boreal—Mature Black Spruce	CA-Obs	53.99	−105.12	ENF	−0.20	*Jarvis et al.* [1997]
Western Boreal—Mature Aspen	CA-Oas	53.62	−106.2	DBF	−0.70	*Blanken et al.* [1997]
Eastern Boreal—Mature Black Spruce	CA-Qfo	49.69	−74.34	ENF	−1.37	*Bergeron et al.* [2007]
Groundhog River Mixedwood	CA-Gro	48.21	−82.16	MF	−1.30	*Coursolle et al.* [2006]
Sylvania Wilderness Area	US-Syv	46.24	−89.35	MF	0.12	*Tang et al.* [2008]
Willow Creek	US-Wcr	45.81	−90.08	DBF	−0.68	*Davis et al.* [2003]
Univ. of Mich. Biological Station	US-UMB	45.56	−84.71	DBF	−0.75	*Schmid* [2003]
Howland Forest (Main Tower)	US-Ho1	45.2	−68.74	ENF	−0.97	*Hollinger et al.* [2004]
Black Hills	US-Blk	44.16	−103.65	ENF	−1.00	*Wilson and Meyers* [2007]
Silas Little—New Jersey	US-Slt	39.91	−74.6	DBF	−0.89	*Clark et al.* [2010]
Morgan Monroe State Forest	US-MMS	39.32	−86.41	DBF	0.19	*Schmid et al.* [2000]
Missouri Ozark Site	US-MOz	38.74	−92.2	DBF	−0.84	*Gu et al.* [2006]
Duke Forest—Hardwoods	US-Dk2	35.97	−79.1	DBF	−0.70	*Pataki and Oren* [2003]
Walker Branch Watershed	US-WBW	35.96	−84.29	DBF	−0.50	*Wilson and Meyers* [2007]
Chestnut Ridge	US-ChR	35.93	−84.33	DBF	−1.13	*Wilson and Meyers* [2007]
Mountainair Pinyon-Juniper Woodland	US-Mpj	34.44	−106.24	WSA	−1.07	*Anderson-Teixeira et al.* [2011]
Rebio Jaru forest	n/a	−10.07	−61.93	EBF	0.61	*von Randow et al.* [2004]

[a]The surface inversion, Γ, was standardized to 10 m above the displacement height. The Γ was calculated individually for each site, except for the Fazenda Nossa Senhora cattle ranch and the Rebio Jaru forest, where Γ was estimated using the values reported in *von Randow et al.* [2004].

2. Methods

2.1. Data Sources

To investigate the biophysical drivers of the surface temperature response to deforestation, this analysis incorporates global satellite and reanalysis data, as well as measurements from a network of flux towers. For our satellite data analysis, we utilized data products from the Moderate Resolution Imaging Spectroradiometer (MODIS), including MODIS-Collection 5 products of land surface temperature (T_S), land cover classification, latent heat flux (*LE*), and white-sky albedo (α) from the years 2003 to 2013. For T_S, we used the 8 day average product (MYD11A2) [*Wan*, 2008] from the Aqua satellite, which contains a daytime (~13:30 local time) and a nighttime (~01:30 local time) measurement, approximating the times of daily maximum and minimum temperatures. We limit our analysis to include only the data that the associated Quality Control (QC) flags indicated to have an average error of ≤1 K. The MODIS ET product (MOD16) is calculated as a combination of soil evaporation, canopy evaporation, and plant transpiration [*Mu et al.*, 2011]. While the land cover type does have a direct influence on the behavior of the MODIS ET, the ET is also strongly constrained by the MODIS fractional photosynthetically active radiation, albedo, and leaf area index products and by the meteorological inputs from the reanalysis data. White-sky albedo (MCD43B3) was obtained at 8 day intervals, a product from both Aqua and Terra satellites, which has a bias mostly less than 5% [*Schaaf et al.*, 2002]. The MODIS land cover classification (MCD12Q1) is produced on an annual basis. We used the primary classification scheme, defined by the International Geosphere-Biosphere Programme (IGBP), which has a typical

accuracy across all classes of 75% for a single year [*Friedl et al.*, 2010], to distinguish forests from nonforested pixels. From the 11 years of data, we created a single land cover map, selecting the dominant land cover type across all years as the primary land cover.

Data from the Modern Era Retrospective-Analysis for Research and Applications (MERRA) [*Rienecker et al.*, 2011] include monthly 2 m air temperature and incoming solar radiation at the surface, as well as hourly surface temperature and 10 m air temperature for the years 2003–2013. The MERRA data were downloaded at a spatial resolution of 1/2° latitude by 2/3° longitude. From the hourly data, we used a single hour, 01:30 local time, to agree with the overpass time of the satellite observations. Similarly, for integration with the satellite data, the MERRA products were screened to include only clear sky conditions.

We collected observational data from 32 flux towers in the United States, Canada, Australia, Brazil, and Germany (Table 1) from the FLUXNET15 Tier 1 data set (http://fluxdata.org/data/fluxnet2015-data-set/) and the Ameriflux database [*Baldocchi et al.*, 2001]. Flux tower sites were selected under the criteria that they had at least 1 year of available data, they had measurements of longwave radiation, and they were situated in a location classified as either grassland or forest. Of these sites, 15 were classified as grassland, and 17 were classified as forest (deciduous, conifer, or mixed forest). With the exception of a single site (site ID: US-MMS), which has hourly measurements, the flux tower data are reported at 30 min intervals. From this half-hourly or hourly data, we selected an hour of data (01:00 local time) to coordinate with the satellite observations and reanalysis data. From these 32 sites, we used the longwave radiation components to calculate radiative surface temperature (discussed in more detail in the next section) and air temperature above the canopy. Two site pairs, each consisting of adjacent forest and grassland towers (US-Dk1 and US-Dk2 [*Novick et al.*, 2004; *Pataki and Oren*, 2003]; US-Seg and US-Mpj [*Anderson-Teixeira et al.*, 2011]), were included in these 32 flux sites. In addition to these 32 sites, we calculated the 01:00 (LST) above-canopy air temperature gradient for five tower sites (Table S2 in the Supporting Information), where air temperature was measured at multiple heights above the canopy (three forest, two grassland).

2.2. Analysis Methodology

We use the space-for-time approach, comparing T_S and the biophysical drivers of the T_S response to deforestation over geographical space, rather than over time (Figure 1). We created 0.5° latitude × 0.5° longitude grids, calculating the average T_S, LE, and albedo for both forests and open land pixels within each grid. Using the IGBP land cover classification scheme, forests were defined using the five forest classes, while open lands were defined as one of three land cover classes: savanna, grasslands, and cropland/natural vegetation mosaic (Table S1). The definition of open land and forest classes were chosen to obtain a broader spatial distribution of grid cells than what would have been available for individual land cover classes. The 0.5° analysis window was chosen as it provided the greatest number of analysis grids with useful data while ensuring similar meteorological influences. Smaller analysis windows reduced down the number of analysis grids that met all the criteria to be included in the final analysis.

We calculated the space-for-time deforestation signal as Δ = open-forest. For all 0.5° × 0.5° grids that contained both forest and open-land cover pixels, we obtained values for day and nighttime ΔT_S (K), ΔLE (W m^{-2}), and $\Delta\alpha$ (dimensionless). We corrected any elevation biases using the Shuttle Radar Topography Mission (SRTM) Global Digital Elevation Model (DEM) at 1 km resolution (SRTMGL30). To remove temperature differences in the 1 km pixels due to elevation differences, all 1 km pixels in the 0.5° analysis grid were adjusted to the mean elevation of the analysis grid using an elevation correction. As the environmental temperature gradient with elevation of the analysis grid was unknown, the temperature to elevation relationships were calculated for each land cover type separately and then combined to give a single analysis grid temperature elevation gradient which was applied to each of the pixels for that time period. This prevented assumptions as to the environmental temperature gradients where inversions or complex topography deviated from average climate lapse rates.

The MERRA data was regridded to 0.5° × 0.5° to correspond to the satellite data grid resolution. The incoming solar radiation data ($K{\downarrow}$) was used to calculate the difference in absorbed solar radiation between forests and nonforested pixels ($\Delta K_a = K{\downarrow}(1 - \Delta\alpha)$). This calculation allows us to directly compare the relative importance of albedo and latent heat flux on ΔT_S. We define a heating potential term as the difference in absorbed solar
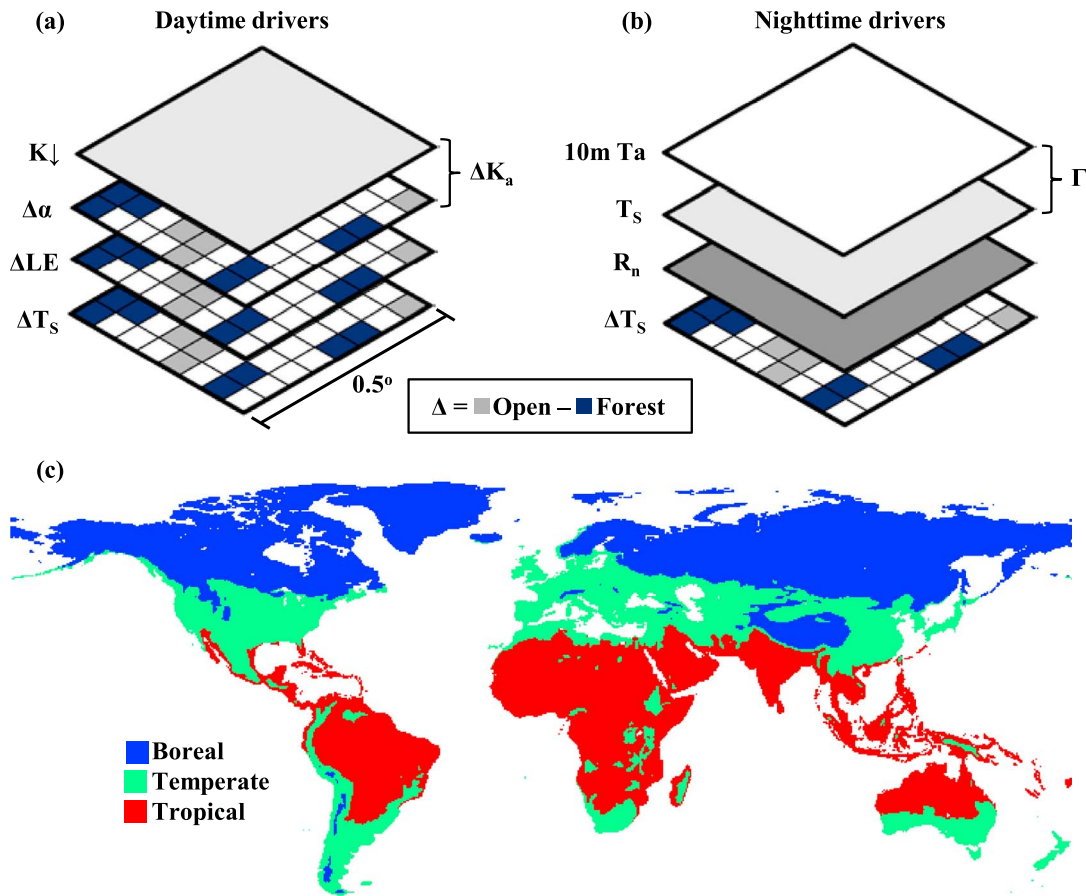
Figure 1. A schematic of the data sources used to investigate the (a) daytime and (b) nighttime drivers of ΔT_S and (c) the geographic extent of the three broad climate zones defined using the MERRA 2 m air temperature data.

radiation and latent heat fluxes between open and forested lands ($\Delta H_P = \Delta K_a - \Delta LE$). The ΔH_P combines two daytime drivers and is a measure of the energy available to warm or cool the surface [*Li et al.*, 2015]. Forests generally have a lower albedo than open lands, absorbing more solar radiation than adjacent nonforested areas. Therefore, a positive ΔH_P indicates that open lands have excess energy compared to forests, and a negative ΔH_P indicates that open lands have a lower energy load compared to forests. Although the ΔH_P does not account for all terms of the surface energy budget, it allows us to directly compare the relative effects of albedo and latent heat flux differences on the surface temperature response to deforestation.

MERRA 01:30 surface temperature and 10 m air temperature were used to calculate the nocturnal surface temperature inversion. We define the surface temperature inversion as the difference between MERRA T_S and 10 m T_a ($\Gamma = T_S - 10\ m\ T_a$). The 10 m T_a is defined by MERRA as 10 m above the displacement height ($d \approx 2/3h$), where h is canopy height. We also use flux tower observations to calculate the nocturnal surface inversion, with measurements of air temperature above the canopy and surface temperature, calculated from the longwave radiation components,

$$T_S = \left[\frac{L_\uparrow - (1 - \varepsilon)\, L_\downarrow}{\varepsilon \sigma} \right]^{(1/4)}$$ (1)

where $L_\uparrow$ and $L_\downarrow$ are the upward and downward longwave radiation fluxes, ε is the surface emissivity (assumed here to be 0.98), and σ is the Stefan-Boltzmann constant ($5.67 \times 10^{-8}\ W\ m^{-2}\ K^{-4}$). As the measurement height of air temperature at the tower sites varied, we standardized the air temperature to
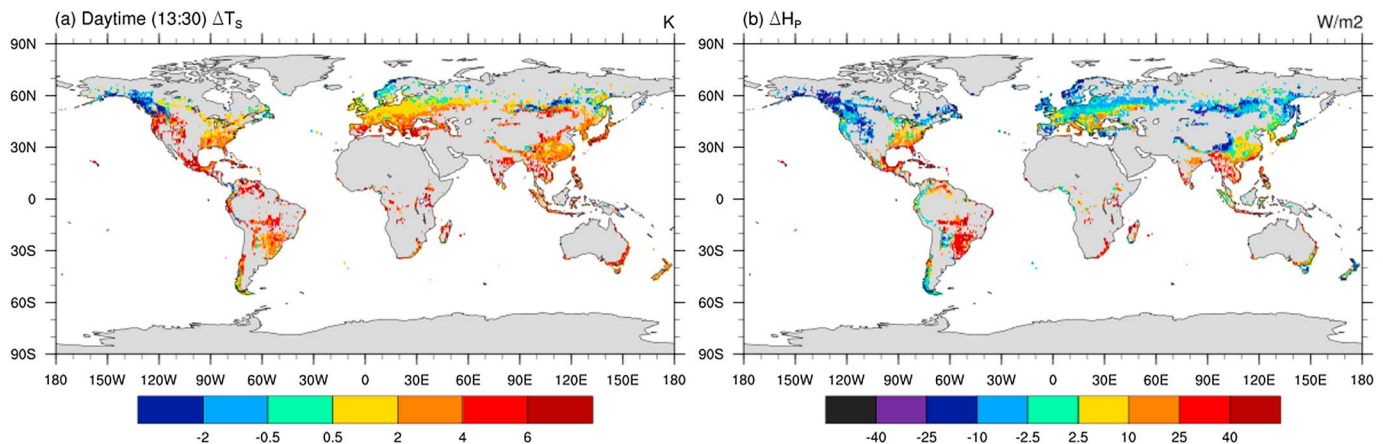
Figure 2. The 11 year annual differences (open-forest) in the (a) daytime surface temperature (ΔT_S) and the (b) heating potential (ΔH_P).

10 m above d using the average nocturnal air temperature gradient from the sites in Table S1 (for further details, see Text S1). The correction of Γ to 10 m above d was small, averaging -0.39 K for grassland sites and 0.34 K for forest sites (Tables S3 and S4).

Finally, as it has been shown that the local response to deforestation depends on background climate [*Li et al.*, 2016, 2015; *Pitman et al.*, 2011], we used the monthly 2 m air temperature from MERRA to define three general climate zones (Figure 1). We define the boreal zone as grids that have an 11 year average of 2 m $T_a < 3.5°C$. The tropical region is defined with annual 2 m temperatures $>24.0°C$. The temperate region is defined as the transitional zone between the tropical and boreal regions, with average annual T_a between 3.5 and 24.0°C. The temperature thresholds were chosen to highlight the differences in the surface temperature response to deforestation across distinct geographical regions, in an analogous method to previous studies that summarize geographical patterns using latitudinal bands [*Lee et al.*, 2011; *Li et al.*, 2015; *Zhang et al.*, 2014]. Our tropical and boreal regions are in general agreement with the tropical (A) and cold (D) climate zones from the Köppen-Geiger climate classification system [*Peel et al.*, 2007]. Although our tropical and boreal zones are farther reaching than the Köppen zones in some regions such as northern Africa and the Tibetan Plateau, we do not include satellite data from those regions because the land cover types that we are examining in this study do not coexist.

3. Results

3.1. Patterns and Drivers of Daytime ΔT_S

Over most regions of the world, open lands are warmer than forests during midday (13:30), with the strongest warming in dry regions (western United States) and in the tropics, where ΔT_S can reach 6 K and above (Figure 2a). At high latitudes ($> \sim 50°N$) in western North America and central Asia, open lands are cooler than forests by up to 2 K. The magnitude of zonal mean ΔT_S follows a latitudinal pattern, with strong warming in low latitudes and slight cooling in high latitudes in the northern hemisphere (Figure 3a). Averaged across climate zones, the average daytime ΔT_S for the tropical, temperate, and boreal zones is 4.4 ± 0.07, 3.1 ± 0.06, and 1.4 ± 0.10 K, respectively. The parameter bounds here and following represent the 95% confidence intervals of the mean difference in each climate zone. The ΔH_P follows a similar pattern to ΔT_S, with large positive values in tropical regions and negative values at high latitudes (Figure 2b). However, the sign of ΔT_S and ΔH_P do not agree in all regions. First, ΔT_S only becomes negative at high latitudes ($> \sim 50°N$), whereas ΔH_P changes sign from positive to negative in the temperate region, as low as 20–30°N (Figure 3b). Second, in arid or semiarid regions (i.e., western United States, southern Europe, and the Middle East), there is a large positive ΔT_S, while the ΔH_P is negative.

We can further investigate the pattern of ΔH_P by examining the magnitude and spatial pattern of the difference in absorbed shortwave radiation (ΔK_a) and latent heat flux (ΔLE) separately. Comparing the magnitudes of ΔK_a and ΔLE allows us to determine the relative importance of each biophysical process to the surface
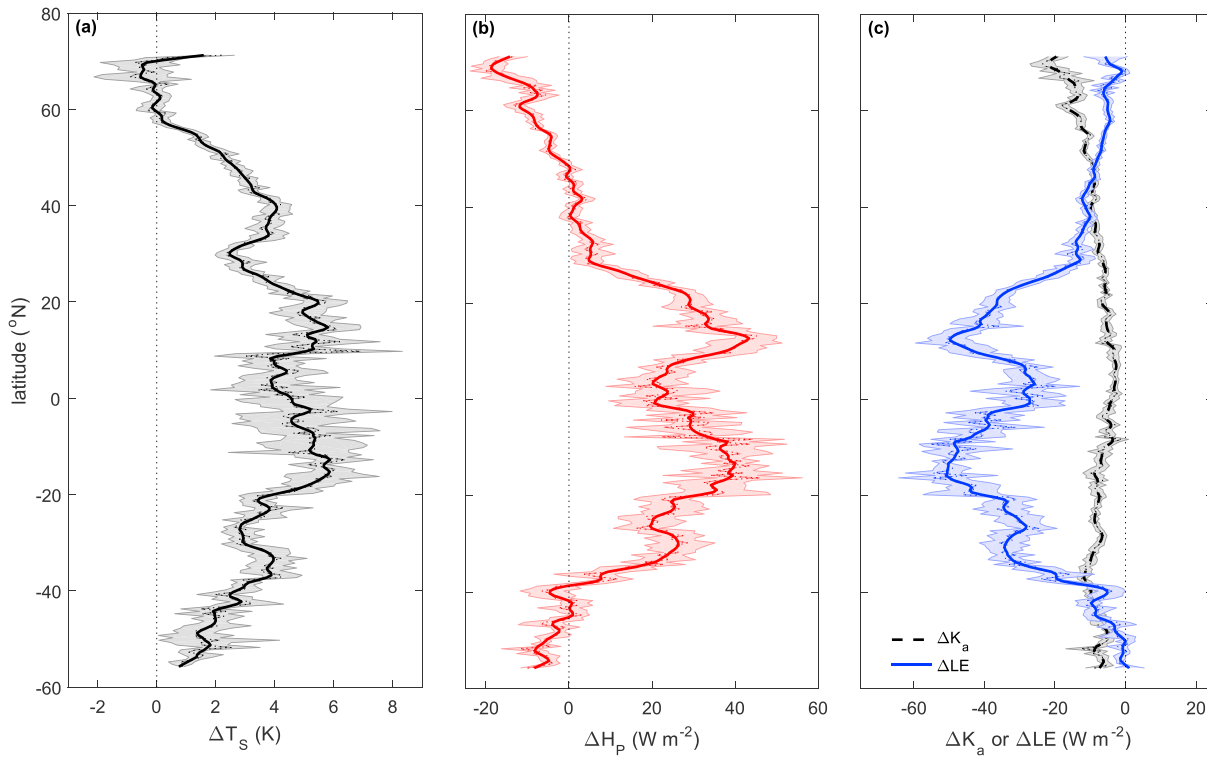
Figure 3. The 11 year annual zonal mean of the differences in the (a) daytime surface temperature (ΔT_S), (b) heating potential (ΔH_P), and (c) the absorbed shortwave radiation (ΔK_a) and the latent heat flux (ΔLE). The shaded regions represent the 95% confidence intervals, and for clarity, the tick lines show the running mean of the zonal data.

energy budget (Figures 3c and S1). Over most latitudes, the magnitude of ΔLE is larger than that of ΔK_a, showing that although open lands absorb slightly less solar radiation, which would result in relative cooling, their surface cooling through latent heat release is much smaller, resulting in overall warming. The largest contrast between these two biophysical processes is in the tropics and that difference gradually decreases with latitude. At high latitudes (~50°N/S), ΔK_a becomes more important than ΔLE. Here, the reduction in absorbed solar radiation is the dominant process, leading to a local cooling response to deforestation. Averaged across the climate zones, the annual ΔK_a for the tropical, temperate, and boreal regions is -5.6 ± 0.17, -7.8 ± 0.11, and -13.2 ± 0.22 W m^{-2}, respectively. In the temperate and boreal zones, these differences are amplified during the winter season, because forests mask the high albedo of snow (Table 2). The annual ΔLE for the tropical, temperate, and boreal regions is -38.2 ± 0.71, -14.0 ± 0.29, and -6.0 ± 0.17 W m^{-2}. A seasonal cycle exists in ΔLE in the temperate and boreal zones, where the contrast is larger during summer months (Table 2).

It is clear that both biophysical processes contribute to ΔT_S, although their relative importance varies geographically. We find that ΔT_S is positively correlated ($R^2 = 0.17$, $p < 0.001$) with ΔK_a (Figure S2a) and negatively correlated ($R^2 = 0.22$, $p < 0.001$) with ΔLE (Figure S2b). Combining these processes into the single ΔH_P term ($\Delta H_P = \Delta K_a - \Delta LE$) allows us to compare the net effect of these two competing processes. We find that there

Table 2. Annual Mean and Seasonal Statistics for Daytime ΔT_S and Drivers

	13:30 ΔT_S (K)			ΔK_a (W m^{-2})			ΔLE (W m^{-2})			ΔH_P (W m^{-2})		
Climate Zone	Annual	JJA	DJF	Annual	JJA	DJF	Annual	JJA	DJF	Annual	JJA	DJF
Boreal	1.4	3.1	−0.9	−13.2	−8.9	−15.9	−6.0	−11.7	0.0	−7.2	2.8	−15.9
Temperate	3.1	3.7	2.0	−7.8	−8.2	−7.9	−14.0	−19.6	−7.3	6.2	11.4	−0.6
Tropical	4.4	4.0	4.2	−5.4	−4.5	−5.9	−38.2	−31.7	−38.1	32.8	27.2	32.2
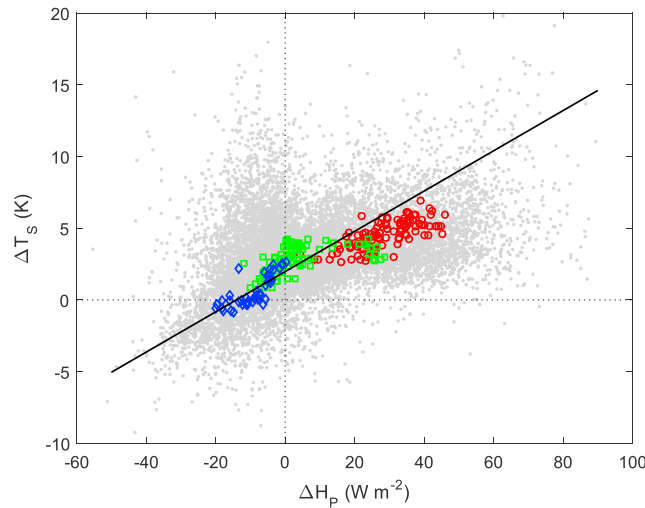
Figure 4. The daytime ΔT_S is positively correlated with heating potential ΔH_P (= $\Delta K_a - \Delta LE$): $y = 0.140(\pm 0.002)x + 1.973(\pm 0.01)$ ($R^2 = 0.27$, $p < 0.001$). Parameter bounds in the regression are for the 95% confidence intervals. As ΔH_P is a measure of the energy available to heat the surface, a positive ΔH_P indicates that grasslands have more energy to warm the surface than trees (and vice versa for a negative ΔH_P). If ΔT_S were influenced only by ΔK_a and ΔLE, the intercept of the regression should go through the origin point. The offset of nearly 2 K likely points to the contribution of differences in roughness/convection efficiency between open lands and trees.

is a positive relationship between ΔH_P and ΔT_S ($R^2 = 0.27$, $p < 0.001$; Figure 4), and it explains the spatial variance in ΔT_S better than ΔK_a or ΔLE alone.

If ΔT_S was only influenced by ΔK_a and ΔLE, then ΔT_S should exactly follow the pattern of ΔH_P: ΔT_S would always be positive where ΔH_P is positive (and vice versa), and the intercept of the regression would go through the origin point. While this significant relationship shows that ΔK_a and ΔLE are major drivers of ΔT_S, the offset of the y intercept of nearly 2 K from zero indicates the contribution of other surface processes to ΔT_S. Surface roughness is the third biophysical process that is known to influence the surface temperature response to deforestation. The larger aerodynamic roughness of forests allows them to more effectively dissipate sensible heat from the surface to the atmosphere. The 2 K of warming

above what the ΔH_P predicts is likely due to differences in surface roughness between the open lands and forests.

3.2. Patterns and Drivers of Nighttime ΔT_S

In contrast to daytime ΔT_S, the nighttime (01:30) ΔT_S is negative over most regions, indicating that open lands are cooler than forests overnight (Figure 5a). The strongest cooling is observed at high latitudes (Figure 6a). In contrast to high latitudes, a slight warming occurs in the tropics. The average ΔT_S across the entire tropical zone is 0.2 ± 0.05 K, while the average ΔT_S in the temperate and boreal zones is -0.7 ± 0.03 K and -1.4 ± 0.04 K, respectively (Table 3). During the night, with no solar radiation and negligible ET, we examine the hypothesis that forests may be warmer because their larger roughness can generate turbulence in the stable atmosphere, bringing warmer air aloft down to the surface. The nighttime ΔT_S does follow a similar
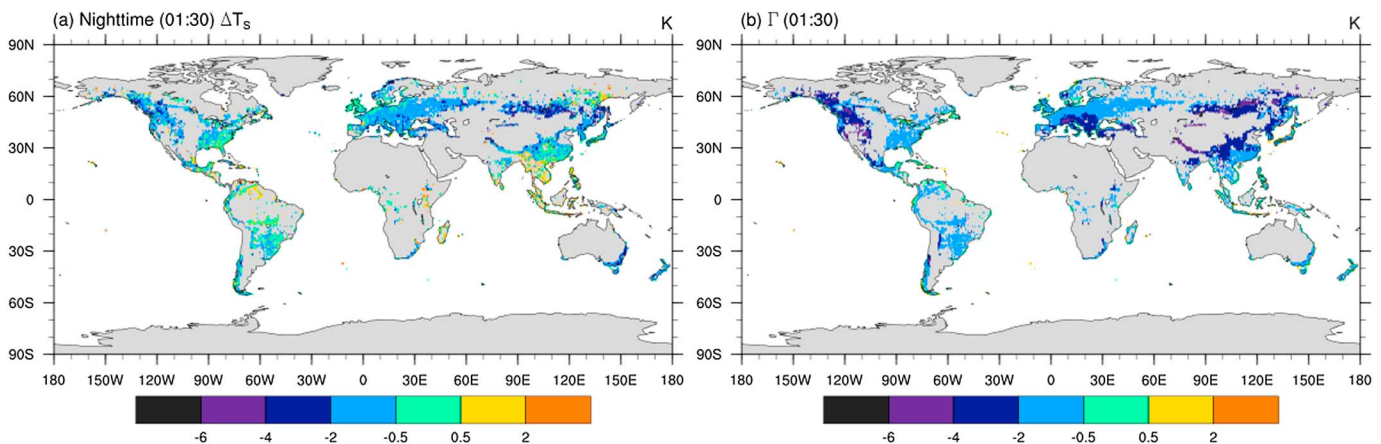
Figure 5. The 11 year annual (a) nighttime ΔT_S and (b) the surface temperature inversion (Γ, MERRA $T_S - 10$ m T_a).
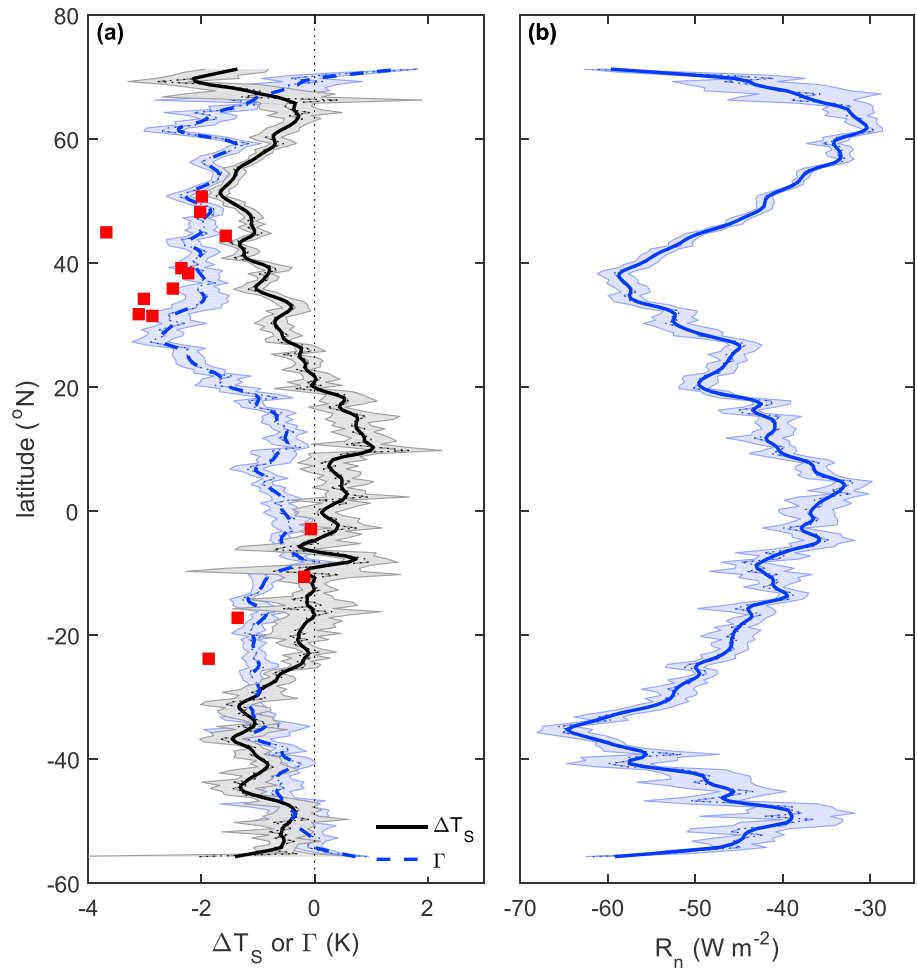
Figure 6. Annual (11 year) zonal means for (a) nighttime ΔT_S and inversion strength Γ, and (b) net radiation, $R_n = L\uparrow - L\downarrow$. The shaded regions represent the 95% confidence intervals, and the thick lines show the running mean of the zonal data. The red squares in Figure 6a display the Γ, standardized to 10 m above the displacement height, from the grassland flux tower sites.

pattern of the surface temperature inversion, Γ (Figures 5b and 6a). The strength of the inversion ranges from -0.9 ± 0.02 K in the tropical zone to -1.5 ± 0.02 K and -2.3 ± 0.02 K in the temperate and boreal zones, respectively. Nighttime ΔT_S and Γ are enhanced in the mid to high latitudes during winter months, with the average ΔT_S reaching -1.9 K and Γ reaching -2.9 K in the boreal zone.

In situ measurements support the latitudinal pattern of Γ (Figure 6a). Calculated from flux tower measurements of T_S and T_a (standardized to 10 m above d), the Γ above open lands is stronger in high latitudes than it is in the tropics. We choose the sites classified as grassland or cropland for comparison with MERRA in Figure 6a because they represent the larger spatial pattern of the nocturnal inversion, unlike forest sites, which, according to our hypothesis, may generate turbulence under stable nighttime conditions, thus

Table 3. Annual Mean and Seasonal Statistics for Nighttime ΔT_S and Drivers

Climate Zone	01:30 ΔT_S (K)			Γ (K)			R_n (W m^{-2})		
	Annual	JJA	DJF	Annual	JJA	DJF	Annual	JJA	DJF
Boreal	−1.4	−0.8	−1.9	−2.3	−2.0	−2.9	−38.3	−41.9	−32.2
Temperate	−0.7	−0.5	−0.9	−1.5	−1.5	−1.6	−48.8	−49.5	−47.6
Tropical	0.2	0.3	0.2	−0.9	−0.8	−1.1	−43.0	−42.0	−44.6
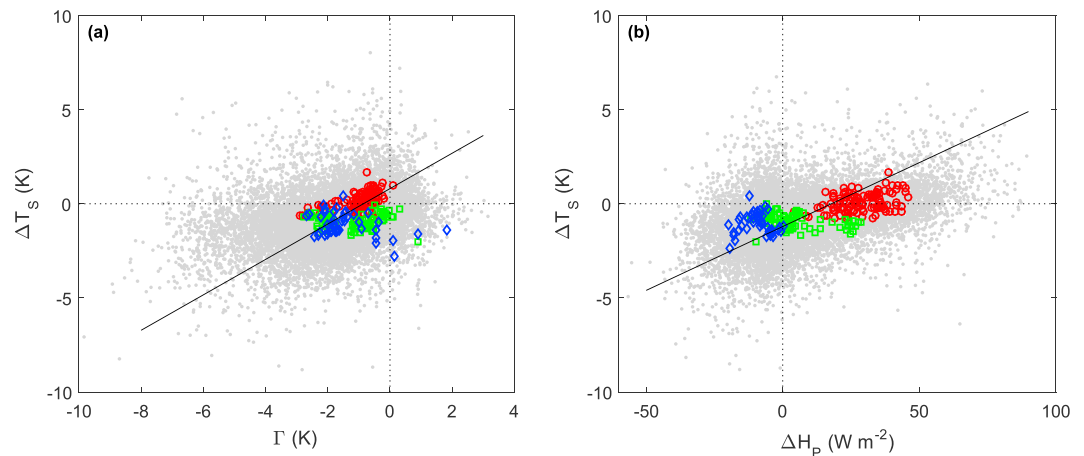
Figure 7. The nighttime ΔT_S is positively correlated with (a) the inversion strength Γ and (b) the heating potential ΔH_P. All data points in Figures 7a and 7b are shown as the gray dots, while the zonal means of each climate zone are shown as the red circles (tropical), green squares (temperate), and blue diamonds (boreal). The black solid lines in (a) $y = 0.941(\pm0.014)x - 0.806(\pm0.023)$ ($R^2 = 0.14$, $p < 0.001$) and (b) $y = 0.068(\pm0.001)x - 1.208(\pm0.006)$ ($R^2 = 0.19$, $p < 0.001$) represent the geometric mean regression for all sample grids (gray dots). Parameter bounds in the regression are for the 95% confidence intervals.

affecting the nocturnal vertical temperature profile. With the exception of a tower site (US-KUT, lat = 45.0°N, $\Gamma = -3.45$ K), the observations of Γ agree relatively well with the MERRA data. However, this outlier may be partially explained by the fact that the measurements were taken over a turfgrass field within a first-ring sub-urb of a major metropolitan area (Minneapolis-St. Paul, Minnesota, USA) [*Hiller et al.*, 2010]. Surface and air temperature at this site may have been influenced by anthropogenic heat sources including vehicle exhaust and residential heating and cooling systems. The strength of the inversion across these open sites ranges from -0.14 to -2.99 K, if excluding the suburban outlier (Table 1), resulting in a mean Γ of -1.93 K across all sites. In contrast, the surface inversion was much weaker over 17 forest sites, ranging from -1.37 to 0.61 K, resulting in a mean Γ of -0.66 K (Table 1). This shows that averaged across similar latitudes, site mea-surements support the hypothesis of forest warming via enhanced vertical mixing of a stable nighttime atmosphere. Further, within this network of flux towers, we collected two "site pairs," each consisting of a set of a forest site and a grassland site, situated in close proximity to each other. Each of these site pairs can be expected to be exposed to similar atmospheric conditions. For the site pair in North Carolina, USA (Dk1 and Dk2), we found that the Γ (standardized to 10 m above d) above the open and forested sites was -2.52 and -0.73 K, respectively. For the pair in New Mexico, USA (Seg and Mpg), the Γ for the open and forested sites were -2.62 and -1.07 K (Figure S3).

There is a positive relationship ($R^2 = 0.14$, $p < 0.001$) between Γ and nighttime ΔT_S (Figure 7a). That the most pronounced surface cooling from deforestation is correlated with strong nighttime surface temperature inversions supports the hypothesis that forests are warmer at night because of enhanced turbulence over for-est canopies. The contrast between the magnitudes of warming observed in the tropics compared to higher latitudes relates to the relative strength of the temperature inversion between those regions. The zonal pat-tern of the nighttime net longwave flux (R_n—the difference between outgoing longwave radiation at the sur-face and incoming longwave radiation) indicates increased radiative cooling in the subtropics (~30–40°N/S) (Figure 6b). The zonal mean pattern of nighttime R_n follows that of the Hadley cell circulation. We hypothe-sized that patterns of R_n would drive the nighttime temperature inversion and ΔT_S, and although there is a positive relationship between R_n and ΔT_S (geometric mean regression: $y = 0.122x(\pm0.002) + 4.602 (\pm0.08)$, $p < 0.001$), there is significant scatter around the regression line, resulting in an R^2 of <0.01 (Figure S4).

There is also a positive relationship ($R^2 = 0.19$, $p < 0.001$) between ΔH_P and nighttime ΔT_S (Figure 7b). While ΔH_P is only a proxy of heat storage, this significant correlation indicates that heat storage during the day con-tributes to nighttime warming of the land surface. Forests in the boreal region absorb and store more energy than open lands, and the release of this heat during the night causes the forests to be warmer than the open lands. However, the amount of excess heat stored in open lands in the tropics is larger than the heat storage

deficit of open lands in the boreal zone. Despite this, nighttime ΔT_S in the tropics is minimal. This shows that daytime heat storage alone cannot fully explain the spatial patterns of nighttime ΔT_S and highlights the additional influence of forest-generated turbulence on nighttime ΔT_S patterns. Together, using multiple linear regression, Γ and ΔH_P explain 26% of the spatial variance in nighttime ΔT_S ($R^2 = 0.26$, $p < 0.001$).

4. Discussion

This study builds upon the works of others who have used regional and global satellite observations to explore the surface temperature response to deforestation or afforestation [*Alkama and Cescatti*, 2016; *Li et al.*, 2015; *Peng et al.*, 2014]. Our goal was to examine the biophysical processes that drive day and nighttime ΔT_S, using global satellite data in coordination with reanalysis and flux tower observations. Of particular interest in this study was to investigate two hypotheses for the relative nighttime warming of forests compared to open lands: (1) that the larger roughness of forests generates turbulence which brings warm air aloft down to the surface, and (2) that the lower albedo of forests contributes to increased heat storage, which is then released at night. This is the first study to investigate the global pattern of the nocturnal surface inversion and its relation to surface temperature and nighttime ΔT_S.

Our results highlight the diurnal asymmetry in the magnitude and sign of the surface temperature response to deforestation. In the tropics, daytime warming dominates the overall warming signal from deforestation, with minimal difference in surface temperature at night. In contrast, the nighttime ΔT_S dominates the overall pattern of the surface cooling response to deforestation in the boreal zone. These results show the importance of both daytime and nighttime measurements to understand the drivers behind the surface temperature response to deforestation.

Although tropical forests have a lower albedo and therefore absorb more solar radiation than adjacent open lands, they are able to access soil water and maintain a consistent latent heat flux even during a prolonged dry season [*von Randow et al.*, 2004], which results in lower surface temperatures. Our results are in general agreement with *Li et al.* [2015], who showed that the ET of tropical forests is greater than that of open areas by up to 500 mm/yr. Climate models tend to agree that deforestation in the tropics results in a reduction in the latent heat flux [*Lawrence and Chase*, 2010; *Snyder et al.*, 2004]; however, due to the varying implementation and physical representation of land use and land cover change in models, there are inconsistencies in the partitioning of energy into latent and sensible heat fluxes across the annual cycle [*de Noblet-Ducoudré et al.*, 2012].

Previous work has suggested that nighttime warming of forests is largely due to the release of daytime heat storage [*Peng et al.*, 2014]. The energy storage rates of forests can comprise a significant portion of net radiation; however, the largest energy storage rates occur during sunrise and sunset and during rainy or cloudy periods [*Michiles and Gielow*, 2008]. The larger biomass and moisture content of forest canopies would increase the heat capacity of forests, slowing down their cooling rate overnight. However, comparative measurements over a tropical forest and pasture showed that storage rates between a tropical forest and pasture were similar at approximately 01:30 (the time of MODIS overpass) [*von Randow et al.*, 2004]. These results are in line with *Bastable et al.* [1993], who compared the available energy at a tropical forest and clearing site, finding that the difference in available energy (including the change in heat storage) between the sites at 01:00 was approximately 10 W m^{-2} during the dry season and negligible during the wet season. While forest canopies may have a higher moisture content than grasslands, soil water storage is higher in tropical grasslands than under forest canopies. *von Randow et al.* [2004] found that in the upper 2 m of soil, water storage was similar under the tropical forests and pasture sites. In the deeper layers (2–3.4 m), forest soil water storage decreased during the dry season, while the water content under the pasture remained relatively constant. Further, measurements show nighttime canopy heat storage rates in a boreal aspen forest of less than 10 W m^{-2} [*Blanken et al.*, 1997] and nighttime storage rate differences of only 3.1 W m^{-2} between forests and open lands at a boreal site cluster in Saskatchewan [*Lee et al.*, 2011].

Our results show that despite a large positive ΔH_P in the tropics (32.8 W m^{-2}), the nighttime surface temperature difference between open lands and forests is close to zero. In the boreal zone, the ΔH_P is negative (−7.2 W m^{-2}), although to a lesser magnitude than the tropical ΔH_P. Yet, the open lands are 1.4°C cooler than forests at night. All together, these results indicate that the daytime surface energy load is not the only

process contributing to nighttime ΔT_S patterns. We found a statistically significant relationship between the nocturnal surface inversion strength and nighttime ΔT_S. This suggests that forests are able to generate turbulence in the stable nighttime atmosphere, bringing heat aloft to the surface, as was shown for wind turbines in Texas [*Zhou et al.*, 2012]. It should be noted that our results here only examine the relationship between ΔT_S and Γ under clear sky conditions. The presence of clouds would result in increased downwelling longwave radiation, heating the surface and the overlying air. Thus, we would expect to see a reduction in the relative nighttime warming of forests under cloudy conditions. However, additional research would be needed to examine this hypothesis. In situ measurements from flux tower sites also show that the surface inversion is weaker over forest canopies and stronger over grassland sites. We found a statistically significant relationship between the nighttime ΔT_S and net radiation ($R_n = L\uparrow - L\downarrow$). We hypothesized that the latitudinal surface inversion pattern is related to the zonal pattern of $L\downarrow$. This theory is supported by the results of *Li et al.* [2016] who showed a decreasing pattern of $L\downarrow$ from the tropics to higher latitudes, where $L\downarrow$ was approximately 50 W m^{-2} near the equator and 25 W m^{-2} at 60°N. Indeed, the combination of both daytime heating and the surface inversion strength was able to better explain the spatial variations in nighttime ΔT_S than either of these drivers alone.

It is interesting to note that while increased vertical mixing and heat release are both processes that contribute to the warmer nighttime temperature of forests, tropical forests are actually slightly cooler than open lands in some tropical areas (~10–20°N). Although over midlatitudes to high latitudes, the nighttime ET flux and the difference in ET between forests and open lands is minimal, *Li et al.* [2015] showed that tropical forests maintain a higher ET than open lands at night on average by approximately 50 mm yr^{-1}. While this is an order of magnitude less than the daytime difference in ET (~500 mm yr^{-1}), the location of the increased nighttime ET flux occurs directly within the region where we observe the nighttime cooling of forests relative to open lands. This persistent nighttime ET flux may be a potential reason why we observe that open lands are warmer than some tropical forests at night.

Our results underscore the importance of the biophysical effects of land cover change on climate. The spatial pattern and magnitude of ΔT_S are largely in agreement with previous empirical satellite data studies [*Li et al.*, 2015; *Peng et al.*, 2014]. It should be noted, however, that this study focuses on the "potential" impact of deforestation. As these results represent a slice of time, they present the impacts from hypothetical land use change around the world. A recent study by *Li et al.* [2016] compared the potential impacts of deforestation on surface temperature (using a methodology similar to the one used in this study) with the actual impacts, finding that the actual impact of deforestation in most regions is very similar to the potential impact, both in terms of sign and latitudinal pattern. *Alkama and Cescatti* [2016] examined the effects of actual deforestation on surface air temperature, inferred from MODIS LST, between 2003 and 2012 and found that the biophysical effects of forest clearing produced large increases in the annual mean maximum air temperature and slight changes to minimum temperatures. Overall, mean warming occurred across most regions, with the exception of high latitudes. They also found that the sensitivity of surface temperature to land cover change (i.e., forest loss) was 50% greater than it was for air temperature, likely due to the satellite retrievals being limited to clear sky conditions [*Alkama and Cescatti*, 2016].

To the best of our knowledge, the role of vertical mixing in the nighttime warming of forests has not been investigated using a modeling approach, although a similar mechanism has been reported for the urban environment [*Wouters et al.*, 2013]. The results of climate modeling studies regarding the role of land cover change on local climate are generally averaged over daily timescales or longer. *Vanden Broucke et al.* [2015] highlight the importance of distinguishing between day and nighttime climate when evaluating the effects of land cover change in a regional climate model, finding that the nighttime warming of forests in Europe is underestimated. As observations demonstrate the asymmetric diurnal response to land cover change, continued investigations into the representation of land cover change in climate models should differentiate between day and nighttime climate.

5. Conclusions

In this study, we examine the patterns and drivers of the day and nighttime surface temperature response to deforestation (ΔT_S) using global satellite observations, reanalysis data, and in situ observations from flux towers. We find that a diurnal asymmetry exists in both the magnitude and sign of ΔT_S. In terms of

magnitude, there is a larger ΔT_S signal over most regions during midday than compared to at night. The sign of ΔT_S changes from positive to negative in many places around the world, with most regions showing daytime warming and nighttime cooling.

There are distinct differences in the diurnal patterns of ΔT_S across different climate zones. In the tropical region, deforestation results in strong warming during the day but has minimal influence on nighttime ΔT_S. In contrast, deforestation in high latitudes produces a large cooling signal at night, with relatively smaller cooling during the day. The temperate region is a transitional zone, showing moderate warming during the day and moderate cooling at night. The combination of satellite and reanalysis data allowed us to compare the relative importance of two competing biophysical processes: differences in absorbed solar radiation and the latent heat flux. We also provide empirical evidence of the importance of surface roughness on both daytime and nighttime ΔT_S.

We find that daytime ΔT_S is driven by differences in absorbed shortwave radiation (ΔK_a) and latent heat flux (ΔLE). While open lands have a higher albedo, and thus lower K_a, the magnitude of ΔLE generally dominates the spatial pattern of ΔT_S resulting in surface warming from deforestation. In high latitudes, the magnitude of ΔK_a overtakes that of ΔLE, resulting in a surface cooling response to deforestation. There is a positive relationship between the heating potential ($\Delta H_P = \Delta K_a - \Delta LE$) and daytime ΔT_S. From this relationship, we estimate that approximately 2 K is not explained by ΔK_a and ΔLE and is likely due to the difference in surface roughness between forests and open lands. The magnitude and spatial pattern of nighttime ΔT_S is related to the strength of the nocturnal temperature inversion, which is stronger in high latitudes and weaker in the tropics. Therefore, the roughness of forests is responsible for daytime cooling (dissipating heat away from the surface) and nighttime warming (bringing warm air aloft down to the surface). Additionally, nighttime ΔT_S is positively related to the relative amount of heat stored in forests and open lands during the day.

The role of forests, including the biophysical effects of deforestation and reforestation, is increasingly being discussed in terms of climate change mitigation. Because of forests' important role in the global carbon cycle, international climate agreements account for land-based climate mitigation strategies including reforestation and afforestation. However, the biophysical effects of such strategies are not yet taken into account. This study and many others show that forest management strategies for the purpose of climate change mitigation need to consider the biophysical effects, as they have a strong influence on local climate. The growing body of evidence suggests that it is necessary to consider where to implement re/afforestation as a climate mitigation strategy. Avoided deforestation and afforestation in the tropics are the most effective from a climate perspective, as they have the strongest cooling effects.

References

Alkama, R., and A. Cescatti (2016), Biophysical climate impacts of recent changes in global forest cover, *Science*, *351*(6273), 600–604.

Anderson-Teixeira, K. J., J. P. Delong, A. M. Fox, D. A. Brese, and M. E. Litvak (2011), Differential responses of production and respiration to temperature and moisture drive the carbon balance across a climatic gradient in New Mexico, *Global Change Biol.*, *17*(1), 410–424, doi:10.1111/j.1365-2486.2010.02269.x.

Anderson, R. G., et al. (2011), Biophysical considerations in forestry for climate protection, *Front. Ecol. Environ.*, *9*(3), 174–182, doi:10.1890/090179.

Bala, G., K. Caldeira, M. Wickett, T. J. Phillips, D. B. Lobell, C. Delire, and A. Mirin (2007), Combined climate and carbon-cycle effects of large-scale deforestation, *Proc. Natl. Acad. Sci. U.S.A.*, *104*(16), 6550–6555, doi:10.1073/pnas.0608998104.

Baldocchi, D., et al. (2001), FLUXNET: A new tool to study the temporal and spatial variability of ecosystem-scale carbon dioxide, water vapor, and energy flux densities, *Bull. Am. Meteorol. Soc.*, *82*(11), 2415–2434, doi:10.1175/1520-0477(2001)082<2415:fantts>2.3.co;2.

Bastable, H. G., W. J. Shuttleworth, R. L. G. Dallarosa, G. Fisch, and C. A. Nobre (1993), Observations of climate, albedo, and surface radiation over cleared and undisturbed Amazonian forest, *Int. J. Climatol.*, *13*, 783–796.

Bergeron, O., H. A. Margolis, T. A. Black, C. Coursolle, A. L. Dunn, A. G. Barr, and S. C. Wofsy (2007), Comparison of carbon dioxide fluxes over three boreal black spruce forests in Canada, *Global Change Biol.*, *13*(1), 89–107, doi:10.1111/j.1365-2486.2006.01281.x.

Beringer, J. (2013), Sturt Plains OzFlux tower site, OzFlux: Australian and New Zealand Flux Research and Monitoring, hdl:102.100.100/14230.

Betts, R. A. (2000), Offset of the potential carbon sink from boreal forestation by decreases in surface albedo, *Nature*, *408*, 187–190.

Blanken, P. D., T. A. Black, P. C. Yang, H. H. Neumann, Z. Nesic, R. Staebler, G. den Hartog, M. D. Novak, and X. Lee (1997), Energy balance and canopy conductance of a boreal aspen forest: Partitioning overstory and understory components, *J. Geophys. Res.*, *102*(D24), 28,915–28,927, doi:10.1029/97JD00193.

Bonan, G. B. (2008), Forests and climate change: Forcings, feedbacks, and the climate benefits of forests, *Science*, *320*(5882), 1444–1449, doi:10.1126/science.1155121.

Clark, K. L., N. Skowronski, and J. Hom (2010), Invasive insects impact forest carbon dynamics, *Global Change Biol.*, *16*(1), 88–101, doi:10.1111/j.1365-2486.2009.01983.x.

Coursolle, C., et al. (2006), Late-summer carbon fluxes from Canadian forests and peatlands along an east–west continental transect, *Can. J. For. Res.*, *36*(3), 783–800, doi:10.1139/x05-270.

Davis, D. J., P. S. Bakwin, C. Yi, B. W. Berger, C. Zhao, R. M. Teclaw, and J. G. Isebrands (2003), The annual cycles of CO_2 and H_2O exchange over a northern mixed forest as observed from a very tall tower, *Global Change Biol.*, 9, 1278–1293.

de Noblet-Ducoudré, N., et al. (2012), Determining robust impacts of land-use-induced land cover changes on surface climate over North America and Eurasia: Results from the first set of LUCID experiments, *J. Clim.*, 25(9), 3261–3281, doi:10.1175/jcli-d-11-00338.1.

Friedl, M. A., D. Sulla-Menashe, B. Tan, A. Schneider, N. Ramankutty, A. Sibley, and X. Huang (2010), MODIS Collection 5 global land cover: Algorithm refinements and characterization of new datasets, *Remote Sens. Environ.*, 114(1), 168–182, doi:10.1016/j.rse.2009.08.016.

Gilmanov, T. G., L. L. Tieszen, B. K. Wylie, L. B. Flanagan, A. B. Frank, M. R. Haferkamp, T. P. Meyers, and J. A. Morgan (2005), Integration of CO_2 flux and remotely-sensed data for primary production and ecosystem respiration analyses in the Northern Great Plains: Potential for quantitative spatial extrapolation, *Global Ecol. Biogeogr.*, 14(3), 271–292, doi:10.1111/j.1466-822X.2005.00151.x.

Gu, L., T. Meyers, S. G. Pallardy, P. J. Hanson, B. Yang, M. Heuer, K. P. Hosman, J. S. Riggs, D. Sluss, and S. D. Wullschleger (2006), Direct and indirect effects of atmospheric conditions and soil moisture on surface energy partitioning revealed by a prolonged drought at a temperate forest site, *J. Geophys. Res.*, 111, D16102, doi:10.1029/2006JD007161.

Hiller, R. V., J. P. McFadden, and N. Kljun (2010), Interpreting CO_2 fluxes over a suburban lawn: The influence of traffic emissions, *Boundary Layer Meteorol.*, 138(2), 215–230, doi:10.1007/s10546-010-9558-0.

Hollinger, D. Y., et al. (2004), Spatial and temporal variability in forest-atmosphere CO_2 exchange, *Global Change Biol.*, 10(10), 1689–1706, doi:10.1111/j.1365-2486.2004.00847.x.

Jackson, R. B., et al. (2008), Protecting climate with forests, *Environ. Res. Lett.*, 3(4), 044006, doi:10.1088/1748-9326/3/4/044006.

Jarvis, P. G., J. M. Massheder, S. E. Hale, J. B. Moncrieff, M. Rayment, and S. L. Scott (1997), Seasonal variation of carbon dioxide, water vapor, and energy exchanges of a boreal black spruce forest, *J. Geophys. Res.*, 102(D24), 28,953–28,966, doi:10.1029/97JD01176.

Krishnan, P., T. P. Meyers, R. L. Scott, L. Kennedy, and M. Heuer (2012), Energy exchange and evapotranspiration over two temperate semi-arid grasslands in North America, *Agric. For. Meteorol.*, 153, 31–44, doi:10.1016/j.agrformet.2011.09.017.

Lawrence, P. J., and T. N. Chase (2010), Investigating the climate impacts of global land cover change in the community climate system model, *Int. J. Climatol.*, 30(13), 2066–2087, doi:10.1002/joc.2061.

Lee, X., et al. (2011), Observed increase in local cooling effect of deforestation at higher latitudes, *Nature*, 479(7373), 384–387, doi:10.1038/nature10588.

Li, Y., M. Zhao, S. Motesharrei, Q. Mu, E. Kalnay, and S. Li (2015), Local cooling and warming effects of forests based on satellite observations, *Nat. Commun.*, 6, 6603, doi:10.1038/ncomms7603.

Li, Y., N. De Noblet-Ducoudré, E. L. Davin, S. Motesharrei, N. Zeng, S. Li, and E. Kalnay (2016), The role of spatial scale and background climate in the latitudinal temperature response to deforestation, *Earth Syst. Dyn.*, 7(1), 167–181, doi:10.5194/esd-7-167-2016.

Mahmood, R., et al. (2014), Land cover changes and their biogeophysical effects on climate, *Int. J. Climatol.*, 34, 929–953.

Malyshev, S., E. Shevliakova, R. J. Stouffer, and S. W. Pacala (2015), Contrasting local versus regional effects of land-use-change-induced heterogeneity on historical climate: Analysis with the GFDL Earth system model, *J. Clim.*, 28(13), 5448–5469, doi:10.1175/jcli-d-14-00586.1.

Michiles, A. A. D. S., and R. Gielow (2008), Above-ground thermal energy storage rates, trunk heat fluxes and surface energy balance in a central Amazonian rainforest, *Agric. For. Meteorol.*, 148(6–7), 917–930, doi:10.1016/j.agrformet.2008.01.001.

Mu, Q., M. Zhao, and S. W. Running (2011), Improvements to a MODIS global terrestrial evapotranspiration algorithm, *Remote Sens. Environ.*, 115(8), 1781–1800, doi:10.1016/j.rse.2011.02.019.

Novick, K. A., P. C. Stoy, G. G. Katul, D. S. Ellsworth, M. B. Siqueira, J. Juang, and R. Oren (2004), Carbon dioxide and water vapor exchange in a warm temperate grassland, *Oecologia*, 138(2), 259–274, doi:10.1007/s00442-003-1388-z.

Oke, T. R. (1987), *Boundary Layer Climates*, pp. 71–76, Cambridge Univ. Press, Cambridge, U. K.

Pataki, D. E., and R. Oren (2003), Species differences in stomatal control of water loss at the canopy scale in a mature bottomland deciduous forest, *Adv. Water Resour.*, 26(12), 1267–1278, doi:10.1016/j.advwatres.2003.08.001.

Peel, M. C., B. L. Finlayson, and T. A. McMahon (2007), Updated world map of the Koppen-Geiger climate classification, *Hydrol. Earth Syst. Sci.*, 11, 1633–1644.

Peng, S. S., S. Piao, Z. Zeng, P. Ciais, L. Zhou, L. Z. Li, R. B. Myneni, Y. Yin, and H. Zeng (2014), Afforestation in China cools local land surface temperature, *Proc. Natl. Acad. Sci. U.S.A.*, 111(8), 2915–2919, doi:10.1073/pnas.1315126111.

Pielke, R. A., R. Avissar, M. Raupach, A. J. Dolman, X. Zeng, and A. S. Denning (1998), Interactions between the atmosphere and terrestrial ecosystems: Influence on weather and climate, *Global Change Biol.*, 4, 461–475.

Pielke, R. A., et al. (2011), Land use/land cover changes and climate: Modeling analysis and observational evidence, *Wiley Interdiscip. Rev. Clim. Change*, 2(6), 828–850, doi:10.1002/wcc.144.

Pitman, A. J., et al. (2009), Uncertainties in climate responses to past land cover change: First results from the LUCID intercomparison study, *Geophys. Res. Lett.*, 36, L14814, doi:10.1029/2009GL039076.

Pitman, A. J., F. B. Avila, G. Abramowitz, Y. P. Wang, S. J. Phipps, and N. de Noblet-Ducoudré (2011), Importance of background climate in determining impact of land-cover change on regional climate, *Nat. Clim. Change*, 1(9), 472–475, doi:10.1038/nclimate1294.

Post, H., H. J. Hendricks Franssen, A. Graf, M. Schmidt, and H. Vereecken (2015), Uncertainty analysis of eddy covariance CO_2 flux measurements for different EC tower distances using an extended two-tower approach, *Biogeosciences*, 12(4), 1205–1221, doi:10.5194/bg-12-1205-2015.

Rienecker, M. M., et al. (2011), MERRA: NASA's Modern-Era Retrospective Analysis for Research and Applications, *J. Clim.*, 24(14), 3624–3648, doi:10.1175/jcli-d-11-00015.1.

Sakai, R. K., D. R. Fitzjarrald, O. L. L. Moraes, R. M. Staebler, O. C. Acevedo, M. J. Czikowsky, R. D. Silva, E. Brait, and V. Miranda (2004), Land-use change effects on local energy, water, and carbon balances in an Amazonian agricultural field, *Global Change Biol.*, 10(5), 895–907, doi:10.1111/j.1529-8817.2003.00773.x.

Schaaf, C. B., et al. (2002), First operational BRDF, albedo nadir reflectance products from MODIS, *Remote Sens. Environ.*, 83, 135–148.

Schmid, H. P. (2003), Ecosystem-atmosphere exchange of carbon dioxide over a mixed hardwood forest in northern lower Michigan, *J. Geophys. Res.*, 108(D14), 4417, doi:10.1029/2002JD003011.

Schmid, H. P., C. S. B. Grimmond, F. Cropley, B. Offerele, and H.-B. Su (2000), Measurements of CO_2 and energy fluxes over a mixed hardwood forest in the mid-western United States, *Agric. For. Meteorol.*, 103, 357–374.

Schroder, I. (2014), Arcturus Emerald OzFlux tower site, OzFlux: Australian and New Zealand Flux Research and Monitoring, hdl: 102.100.100/14249.

Schultz, N. M., X. Lee, P. J. Lawrence, D. M. Lawrence, and L. Zhao (2016), Assessing the use of subgrid land model output to study impacts of land cover change, *J. Geophys. Res. Atmos.*, 121, 6133–6147, doi:10.1002/2016JD025094.

Snyder, P. K., C. Delire, and J. A. Foley (2004), Evaluating the influence of different vegetation biomes on the global climate, *Clim. Dyn.*, 23(3–4), 279–302, doi:10.1007/s00382-004-0430-0.

Tang, J., P. V. Bolstad, A. R. Desai, J. G. Martin, B. D. Cook, K. J. Davis, and E. V. Carey (2008), Ecosystem respiration and its components in an old-growth forest in the Great Lakes region of the United States, *Agric. For. Meteorol.*, *148*(2), 171–185, doi:10.1016/j.agrformet.2007.08.008.

Thompson, S. E., C. J. Harman, A. G. Konings, M. Sivapalan, A. Neal, and P. A. Troch (2011), Comparative hydrology across AmeriFlux sites: The variable roles of climate, vegetation, and groundwater, *Water Resour. Res.*, *47*, W00J07, doi:10.1029/2010WR009797.

Vanden Broucke, S., S. Luyssaert, E. L. Davin, I. Janssens, and N. van Lipzig (2015), New insights in the capability of climate models to simulate the impact of LUC based on temperature decomposition of paired site observations, *J. Geophys. Res. Atmos.*, *120*, 5417–5436, doi:10.1002/2015JD023095.

von Randow, C., et al. (2004), Comparative measurements and seasonal variations in energy and carbon exchange over forest and pasture in South West Amazonia, *Theor. Appl. Climatol.*, *78*(1–3), 5–26, doi:10.1007/s00704-004-0041-z.

Wan, Z. (2008), New refinements and validation of the MODIS land-surface temperature/emissivity products, *Remote Sens. Environ.*, *112*(1), 59–74, doi:10.1016/j.rse.2006.06.026.

Wickham, J. D., T. G. Wade, K. H. Riitters, and J. Peñuelas (2013), Empirical analysis of the influence of forest extent on annual and seasonal surface temperatures for the continental United States, *Global Ecol. Biogeogr.*, *22*(5), 620–629, doi:10.1111/geb.12013.

Wilson, T. B., and T. P. Meyers (2007), Determining vegetation indices from solar and photosynthetically active radiation fluxes, *Agric. For. Meteorol.*, *144*(3–4), 160–179, doi:10.1016/j.agrformet.2007.04.001.

Winckler, J., C. H. Reick, and J. Pongratz (2017), Robust identification of local biogeophysical effects of land-cover change in a global climate model, *J. Clim.*, *30*(3), 1159–1176, doi:10.1175/jcli-d-16-0067.1.

Wouters, H., K. De Ridder, M. Demuzere, D. Lauwaet, and N. P. M. van Lipzig (2013), The diurnal evolution of the urban heat island of Paris: A model-based case study during summer 2006, *Atmos. Chem. Phys.*, *13*(17), 8525–8541, doi:10.5194/acp-13-8525-2013.

Xu, L., and D. D. Baldocchi (2004), Seasonal variation in carbon dioxide exchange over a Mediterranean annual grassland in California, *Agric. For. Meteorol.*, *123*(1–2), 79–96, doi:10.1016/j.agrformet.2003.10.004.

Zhang, M., et al. (2014), Response of surface air temperature to small-scale land clearing across latitudes, *Environ. Res. Lett.*, *9*(3), 034002, doi:10.1088/1748-9326/9/3/034002.

Zhou, L., Y. Tian, S. Baidya Roy, C. Thorncroft, L. F. Bosart, and Y. Hu (2012), Impacts of wind farms on land surface temperature, *Nat. Clim. Change*, doi:10.1038/nclimate1505.